Giant Topological Insulator Gap in Graphene with 5*d* Adatoms

Jun Hu,[1] Jason Alicea,[1,2,*] Ruqian Wu,[1,†] and Marcel Franz[3]

[1]*Department of Physics and Astronomy, University of California, Irvine, California 92697, USA*
[2]*Department of Physics, California Institute of Technology, Pasadena, California 91125, USA*
[3]*Department of Physics and Astronomy, University of British Columbia, Vancouver, British Columbia V6T 1Z1, Canada*

(Received 29 June 2012; published 27 December 2012)

Two-dimensional topological insulators (2D TIs) have been proposed as platforms for many intriguing applications, ranging from spintronics to topological quantum information processing. Realizing this potential will likely be facilitated by the discovery of new, easily manufactured materials in this class. With this goal in mind, we introduce a new framework for engineering a 2D TI by hybridizing graphene with impurity bands arising from heavy adatoms possessing partially filled *d* shells, in particular, osmium and iridium. First-principles calculations predict that the gaps generated by this means exceed 0.2 eV over a broad range of adatom coverage; moreover, tuning of the Fermi level is not required to enter the TI state. The mechanism at work is expected to be rather general and may open the door to designing new TI phases in many materials.

DOI: 10.1103/PhysRevLett.109.266801 PACS numbers: 73.22.Pr

Topological insulators (TIs) comprise a class of strongly spin-orbit-coupled nonmagnetic materials that are electrically inert in the bulk yet possess protected metallic states at their boundary [1–3]. These systems are promising sources for many exotic phenomena—including Majorana fermions [4–7], charge fractionalization [8], and novel magnetoelectric effects [9–12]—and may also find use for quantum computing [2] and spintronics devices [13]. In some respects, two-dimensional (2D) TIs are ideally suited for such applications; for example, bulk carriers that often plague their three-dimensional counterparts can be vacated simply by gating. Experimental progress on 2D TIs has steadily advanced recently due largely to pioneering work on HgTe [14–17] (see also Ref. [18]). Nevertheless, to realize their full potential, systems more amenable to experimental investigations are highly desirable. In this regard, the ability to design new 2D TIs from conventional materials would constitute a major step forward, and many proposals of this spirit now exist [19–26].

Following this strategy, we introduce a new mechanism for engineering a TI state in graphene—arguably now the most broadly accessible 2D system. Historically, graphene was the first material predicted to realize a TI in a seminal work by Kane and Mele [1], although unfortunately the gap is unobservably small due to carbon's weak spin-orbit coupling (SOC) [27–31]. Reference [23] revived graphene as a viable TI candidate by predicting that dilute concentrations of heavy In or Tl adatoms dramatically enhance the gap to detectable values of the order of 0.01 eV (see also Refs. [32,33]). Essentially, these adatoms mediate enhanced SOC of the type present in the Kane-Mele model [1] for pure graphene.

Our approach here relies on hybridizing graphene with dilute heavy adatoms as in prior studies [23,34,35], although the physics is entirely different and cannot be understood in terms of an effective graphene-only model. Rather, we will show using density functional theory (DFT) that certain adatoms—specifically, Os, Ir, Cu–Os dimers, and Cu–Ir dimers—form spin-orbit-split impurity bands that hybridize with graphene's Dirac states, producing a highly robust TI phase. In fact, here it is more appropriate to view the adatoms as the dominant low-energy degrees of freedom, with *their* coupling effectively mediated by graphene; from this perspective, this mechanism represents the inverse of that invoked in Ref. [23].

Numerous practical advantages arise in this scheme. The TI gaps are extremely large—typically exceeding 0.2 eV—and take on nearly the full *atomic* adatom spin-orbit splitting. Such values reflect more than an order-of-magnitude enhancement compared to the gaps induced by In or Tl and are competitive with the largest gap predicted for any TI. These gaps, moreover, are remarkably insensitive to the adatom concentration, taking on comparable values, at least over coverages ranging from ~2–6%. In the case of Os adatoms and Cu–Ir dimers, the Fermi level also naturally resides within the TI band gap. This eliminates a serious challenge with In and Tl, both of which substantially electron-dope graphene even at quite low coverages. These features suggest that the observation of a TI state in graphene may be within reach.

We first elucidate the mechanism uncovered here using a tight-binding model that exposes the physics in a transparent manner. Consider $5d$ adatoms residing at positions $\mathbf{R}$ located at "hollow" (H) sites in graphene as in Fig. 1(a). For simplicity, we retain only the d_{xz} and d_{yz} adatom states since these comprise the most important orbitals in our first-principles calculations. (Recall that $d_{xz/yz}$ orbitals arise from L^z orbital angular momentum $m = \pm 1$ states.) We then model the composite system by a Hamiltonian $H = H_g + H_a + H_c$ [23]. The first term allows nearest-neighbor hopping for graphene: $H_g = -t\sum_{\alpha=\uparrow,\downarrow}\sum_{\langle \mathbf{r}\mathbf{r}'\rangle}(c^\dagger_{\mathbf{r}\alpha}c_{\mathbf{r}'\alpha} + \text{H.c.})$,

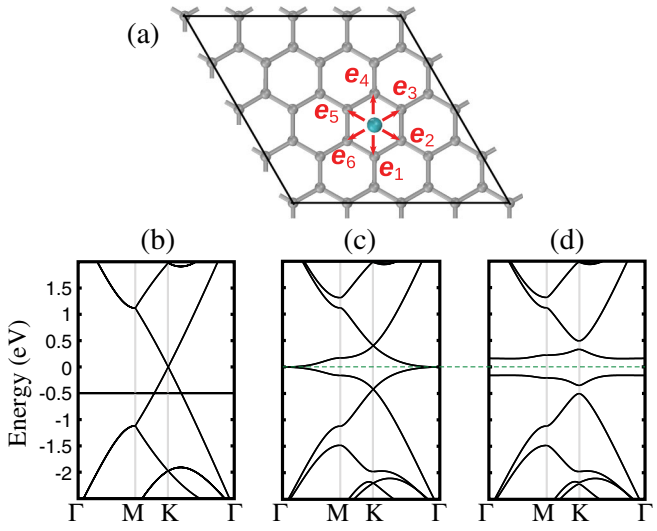

FIG. 1 (color online). (a) 4×4 supercell employed to simulate periodic H-site adatoms (cyan) at 6.25% coverage. (b)–(d) Corresponding tight-binding band structures calculated with graphene hopping strength $t = 2.7$ eV and adatom on-site energy $\epsilon = -0.5$ eV. The adatom-graphene hopping t_c and adatom SOC Λ_{SO} are given by (b) $t_c = \Lambda_{\mathrm{SO}} = 0$; (c) $t_c = 1.5$ eV, $\Lambda_{\mathrm{SO}} = 0$; and (d) $t_c = 1.5$ eV, $\Lambda_{\mathrm{SO}} = 0.2$eV. When the Fermi level sits at the dashed green line, Λ_{SO} generates a giant TI gap.

where $c^\dagger_{\mathbf{r}\alpha}$ adds an electron with spin α to honeycomb site $\mathbf{r}$. The second encodes adatom couplings,

$$H_a = \sum_{\mathbf{R}} \Big[\sum_{\alpha=\uparrow,\downarrow} \sum_{m=\pm 1} \epsilon f^\dagger_{m\mathbf{R}\alpha} f_{m\mathbf{R}\alpha} + \sum_{\alpha,\beta=\uparrow,\downarrow} \Lambda_{\mathrm{SO}} (f^\dagger_{1\mathbf{R}\alpha} s^z_{\alpha\beta} f_{1\mathbf{R}\beta} - f^\dagger_{-1\mathbf{R}\alpha} s^z_{\alpha\beta} f_{-1\mathbf{R}\beta}) \Big]. \quad (1)$$

Here, $f^\dagger_{m\mathbf{R}\alpha}$ fills the adatom d orbital at position $\mathbf{R}$ with magnetic quantum number $m = \pm 1$ and spin α, ϵ sets the orbital energies relative to graphene's Dirac points, Λ_{SO} represents SOC, and s^z is a Pauli matrix. Finally, H_c hybridizes the adatoms with graphene. To express this term, it is convenient to define vectors $\mathbf{e}_j$ that point from an adatom to the six surrounding carbon sites [see Fig. 1(a)]. One can then construct linear combinations $C_{m\mathbf{R}} = \frac{1}{\sqrt{6}} \times \sum_{j=1}^{6} e^{-i(\pi/3)m(j-1)} c_{\mathbf{R}+\mathbf{e}_j}$ that carry angular momentum m and write [23]

$$H_c = -t_c \sum_{\mathbf{R}} \sum_{\alpha=\uparrow,\downarrow} \sum_{m=\pm 1} (i C^\dagger_{m\mathbf{R}\alpha} f_{m\mathbf{R}\alpha} + \mathrm{H.c.}). \quad (2)$$

Let us now specialize to a periodic adatom arrangement characterized by the 4×4 supercell shown in Fig. 1(a), with one adatom per cell (corresponding to 6.25% coverage). Figure 1(b) illustrates the band structure with $t = 2.7$ eV, $\epsilon = -0.5$ eV, and $t_c = \Lambda_{\mathrm{SO}} = 0$. In this limit, the

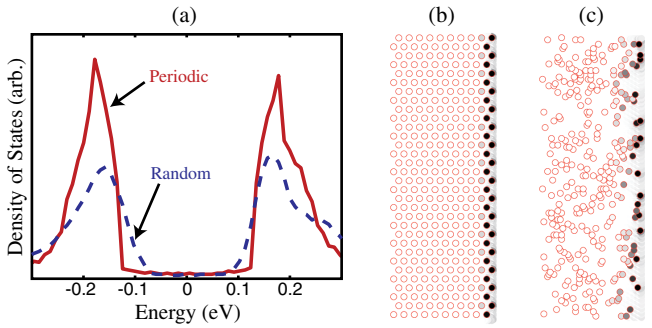

FIG. 2 (color online). (a) Density of states for periodic (solid curve) and random (dashed curve) adatoms at 6.25% coverage on a graphene strip with armchair edges along x and periodic boundary conditions along y. The parameters are the same as for Fig. 1(c). The finite density of states within the bulk gap reflects edge states. Examples of edge states for the periodic and random cases respectively appear in (b) and (c).

adatoms produce a fourfold degenerate flat band, reflecting spin and orbital degeneracy. For the following discussion, the precise location of these adatom states is unimportant, provided they intersect the carbon bands within ~ 1 eV of the Dirac points. Incorporating tunneling between the adatoms and graphene causes the flat bands to disperse, as shown in Fig. 1(c) for $t_c = 1.5$ eV. Suppose now that the Fermi level resides at the dashed line in Fig. 1(c). Although the spectrum here exhibits a sizable energy gap near the K point, the system remains metallic due to band touchings at the zone center. The gapless excitations at zero momentum exhibit the following two crucial properties: (i) they arise from *weakly perturbed adatom orbitals* since at the zone center the nearest carbon bands reside well over 1 eV away and (ii) they are protected by time-reversal, spatial rotation, and SU(2) spin symmetries that coexist when $\Lambda_{\mathrm{SO}} = 0$. Breaking the last of these symmetries by turning on SOC thus produces a bulk gap given nearly by the *atomic* spin-orbit splitting for the adatoms, despite their dilute coverage. This key point is demonstrated in Fig. 1(d) for $\Lambda_{\mathrm{SO}} = 0.2$ eV, which yields a 0.32 eV gap that constitutes 80% of a single adatom's spin-orbit splitting.

The gap opening indeed drives the system into a TI phase. Since our Hamiltonian is inversion symmetric, this can be verified by computing Fu and Kane's formula for the Z_2 invariant in Ref. [36] (details are provided in the Supplemental Material [37]). For additional evidence, the solid curve in Fig. 2(a) plots the density of states (DOS) near zero energy for the same periodic adatom coverage on a graphene strip with armchair edges along x and periodic boundary conditions along y. (Our strip consists of 128 zig-zag "rows" of carbon sites, with 80 sites per row.) Edge states characteristic of the topological phase produce a finite DOS inside of the bulk gap and are clearly resolvable in the system size simulated over an energy window of 0.31 eV. As an example, an edge state with midgap energy $E = 0.004$ eV appears in Fig. 2(b), where circles indicate

adatom locations while the shading represents the probability amplitude extracted from the wave function.

Remarkably, the formation of a TI by no means requires the periodic arrangements considered so far. Similar physics arises even for *completely randomly* distributed H-site adatoms. The dashed curve in Fig. 2(b) illustrates the DOS for the random case, again at 6.25% coverage. Even in our finite system, one can easily resolve edge modes within a 0.21 eV energy range that is comparable to the bulk gap for the periodic case; see e.g., the midgap state with energy $E = 0.003$ eV plotted in Fig. 2(c). Transport calculations for the random case similar to Ref. [23] also reveal conductance quantization expected for the topological phase [38].

Next, we demonstrate using DFT that the mechanism described above can be realized in graphene with $5d$ adatoms, notably Os and Ir. All DFT calculations were carried out with the Vienna *ab initio* simulation package [39,40] at the level of the local density approximation [41], including SOC unless specified otherwise. Most results were obtained using the supercell in Fig. 1(a), with one adatom per cell. See the Supplemental Material [37] for additional details and a comparison with generalized gradient approximation results [35]. Below, we discuss Os and then turn to Ir.

Since the thermal stability of adsorption structures is relevant for both experiments and applications, candidate adatoms should ideally exhibit large H-site binding energies [defined as $E_b = E(\text{graphene}) + E(\text{adatom}) - E(\text{adatom/graphene})$] and high diffusion energy barriers [defined as $\Delta E = E_b(\text{transition state}) - E_b(\text{ground state})$]. Osmium satisfies both criteria. The binding energy for Os at the H site in graphene is 2.42 eV—much larger than the "top" (directly above a C) and the "bridge" (above the midpoint of a C–C bond) configurations for which E_b is 1.70 and 1.59 eV, respectively. Moreover, the calculated diffusion barrier for an Os adatom to diffuse from an H site through the top site is found to equal the difference between the binding energies at these positions, 0.72 eV. The barrier for diffusion through the bridge site is similarly given by 0.83 eV. Therefore, despite the fact that aggregation generally lowers the system's energy, dilute Os adatoms should be stable over H sites even at room temperature. By contrast, most $3d$ transition metals have $E_b \sim 1$ eV [42] and are much more mobile [42,43] and susceptible to clustering; for example, the diffusion barrier is only 0.40 eV for Co on graphene [44].

Figure 3(a) displays the DFT band structure for periodic H-site Os adatoms on graphene at 6.25% coverage using the 4×4 supercell in Fig. 1(a). Each Os adatom forms a charge state of $+0.55e$ (based on the Bader charge division scheme [45]), indicating that the Os–graphene bonds mix covalent and ionic features. Clearly, these bonds dramatically modify the characteristic Dirac bands at the K point of pure graphene similar to Fig. 1. Most importantly, Os induces a band gap $\Delta_{\text{SO}} = 0.27$ eV, *right at the Fermi level* given by the green dashed line in Fig. 3(a). As in our tight-binding model, the gap here results solely from SOC. (Without SOC, a gapless spectrum arises; see the Supplemental Material [37].) More precisely, the partial density of states (PDOS) for the Os $5d$ orbitals displayed in Fig. 3(b) indicates that the gap arises from the hybridization between graphene's π states and the spin-orbit-split d_{xz} and d_{yz} adatom orbitals, also as in our tight-binding model. The PDOS for the d_{z^2}, $d_{x^2-y^2}$ and d_{xy} orbitals, by contrast, is concentrated at much lower energies. Thus, the gap-opening mechanism introduced earlier indeed appears in the realistic Os–graphene system.

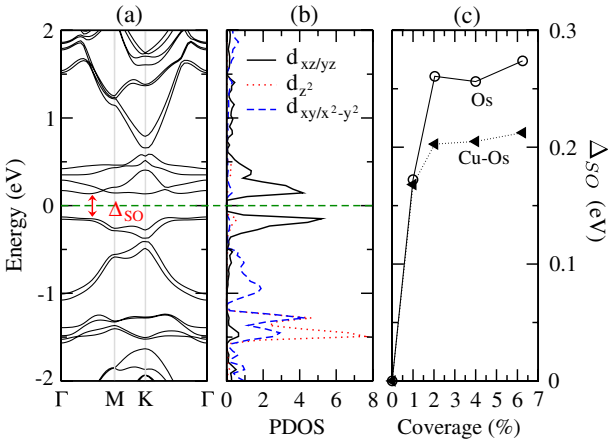

FIG. 3 (color online). (a) First-principles band structure for Os on graphene at 6.25% coverage. The green dashed line indicates the Fermi level. (b) Corresponding PDOS for the Os $5d$ levels. The large gap Δ_{SO} visible in (a) arises from hybridization between graphene and the spin-orbit-split $d_{xz/yz}$ orbitals, as in our tight-binding model. (c) Coverage dependence of the gap for graphene with Os adatoms (circles) and Cu–Os dimers (triangles).

The Os-induced gap depends exceptionally weakly on coverage. To illustrate this point, we performed simulations of graphene with one Os adatom in 5×5, 7×7, and 10×10 supercells (corresponding to coverages of 4, 2.04, and 1%). Circles in Fig. 3(c) show the DFT-predicted gaps, which remain close to 0.2 eV even at 1% coverage. This striking feature is actually rather natural since the local atomic spin-orbit splitting for the Os d_{xz} and d_{yz} orbitals essentially sets Δ_{SO}.

Strictly speaking, a true TI phase does not arise in the DFT simulations described above since Os forms small spin and orbital magnetic moments of $0.45\,\mu_B$ and $0.05\,\mu_B$, respectively. This produces visible splittings of the bands at the Γ and M points corresponding to time-reversal-invariant momenta; see Fig. 3(a). One should keep in mind, however, that DFT can sometimes overestimate moment formation. Nonetheless, even if a moment M_s appears in an experiment, there are practical means by which this can be quenched to zero to reveal a bona fide topological phase. One effective approach is to apply an external electric field ε. Figure 4(a) illustrates that M_s of

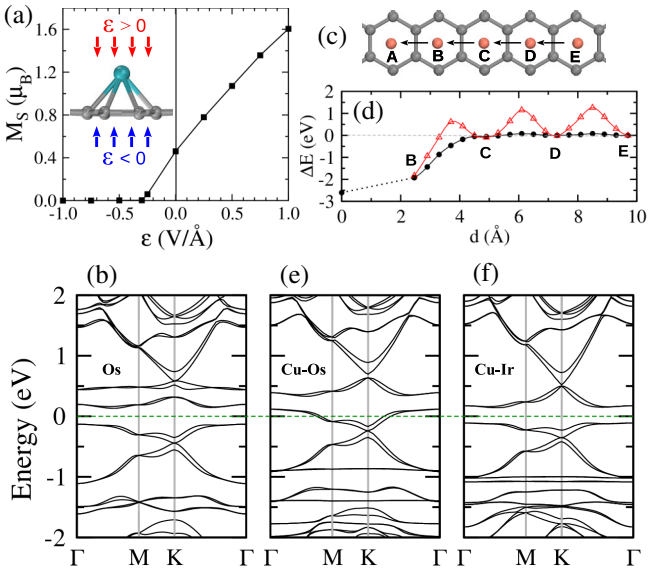

FIG. 4 (color online). (a) Magnetic moment M_s for graphene with Os versus external electric field ε applied perpendicular to the graphene sheet (see the inset for the direction of positive and negative ε). (b) Band structure of an Os–graphene system with $\varepsilon = -0.5$ V/Å corresponding to a vanishing moment. The large gap at the Fermi level (green dashed line) thus reflects a true TI phase. (c) Possible diffusion path of a Cu atom or a Cu–Os dimer, beginning from position E. The Cu atom ends above an Os atom at position A; the Cu–Os dimer ends at position B, adjacent to another Cu–Os dimer at position A. (d) Energy profile for Cu (circles) and the Cu–Os dimer (triangles) along the diffusion trajectory in (c). The small diffusion barrier evident for the Cu atom indicates that Cu–Os dimers should readily form. In contrast, the O(eV) diffusion barrier for the Cu–Os dimer suggests a suppression of clustering at low coverages, even at room temperature. (e) Band structure for Cu–Os dimers on graphene. Time-reversal symmetry is preserved here even at $\varepsilon = 0$, although the Fermi level now resides in the valence band. (f) Band structure for Cu–Ir dimers on graphene. This system preserves time-reversal symmetry, eliminates the shift in Fermi level, and also supports a large TI gap. Coverage in (b), (e), and (f) is 6.25%.

Os on graphene depends sensitively on ε. In particular, $\varepsilon < 0$ transfers additional charge from Os to graphene and kills the moment for $\varepsilon \lesssim -0.3$ V/Å. (Stray fields from charged impurities may somewhat modify this condition.) The electric fields required to restore time-reversal symmetry only weakly affect the band structure. See for example, Fig. 4(b) corresponding to 6.25% Os coverage with $\varepsilon = -0.5$ V/Å, where a time-reversal-invariant TI appears with a gap $\Delta_{SO} = 0.26$ eV.

Codoping provides another means to quench the Os magnetic moment. To preserve the main features of the band structure while attracting charge away from Os (as accomplished by a negative ε), coadsorbates should interact weakly with graphene and exhibit larger electronegativity than Os. Following this guidance, we considered Cu, Ag, and Au in several configurations, as described in the Supplemental Material [37]. Whereas Os repels Ag and Au adatoms, Cu prefers to climb over Os to form a vertical Cu–Os dimer over the H site. The binding energy $E_b = E(\text{graphene}) + E(\text{Cu}) + E(\text{Os}) - E(\text{Cu} - \text{Os}/\text{graphene})$ for these dimers is 5.96 eV, higher by 2.50 eV compared to that of well-separated Cu and Os adatoms. Additionally, Cu more strongly anchors Os to the H site since the binding energy for the vertical dimers over the top (bridge) site is weaker by 1.27 (1.42) eV.

In practice, however, it is also essential that isolated Cu and Os adatoms can readily dimerize without overcoming substantial energy barriers. We explored this issue by computing the energy (without SOC) along the diffusion path depicted in Fig. 4(c), where a Cu adatom beginning at position E ends up above an Os at position A. Figure 4(d) illustrates the energy change ΔE relative to the dimer state along this trajectory. The energy barrier for a Cu adatom moving from location E to B is only ~0.08 eV; once at position B, the Cu strongly attracts to the top of the Os. This suggests that dimer formation ought to proceed quite efficiently. To better appreciate this effect, we also calculated the energy change for two Cu–Os dimers in an 8×8 supercell, one residing at A while the other diffuses from E to B. Large energy barriers exist for all hopping steps: 1.27 eV for $E \rightarrow D$, 1.25 eV for $D \rightarrow C$, and 0.7 eV for $C \rightarrow B$, indicating that Cu–Os dimer diffusion is essentially blocked at low temperature. We thus expect that clustering of dilute $5d$ metal adatoms and dimers on graphene should not be a concern.

Because of the hybridization and charge transfer between the Cu and Os atoms—the Bader charges of Cu and Os are respectively $-0.21e$ and $+0.67e$—DFT predicts that graphene with Cu–Os dimers is nonmagnetic. The spectrum for graphene with Cu–Os at 6.25% coverage again supports a large TI gap $\Delta_{SO} = 0.21$ eV, as is evident in the band structure of Fig. 4(e). Moreover, the triangles in Fig. 3(c) show that this gap exhibits similarly weak coverage dependence, as for Os on graphene. The drawback here, however, is that the Fermi level [green line in Fig. 4(e)] now resides in the valence band. Returning the Fermi level to the insulating regime should be possible with conventional gating techniques, provided one works at low coverage.

Alternatively, the hole introduced by each Cu–Os dimer can be compensated by replacing Os with Ir, which has one additional electron. Our calculations show that vertical Cu–Ir dimers also strongly bind to the H site in graphene without forming a magnetic moment. Hybridization between Cu–Ir dimers and graphene produces nearly the same band structure as for Cu–Os but with the Fermi level lying in the band gap. See the band structure for 6.25% Cu–Ir coverage in Fig. 4(f), where the gap is $\Delta_{SO} = 0.25$ eV. Additional results for Ir on graphene—which behaves similarly to the Os case—can be found in the Supplemental Material [37].

In summary, we have introduced a mechanism by which graphene covered with heavy adatoms realizes a TI protected by a giant gap comparable to atomic spin-orbit energies, even at exceptionally dilute coverages. Using DFT, we predicted that Os, Ir, Cu–Os dimers, and Cu–Ir dimers all give rise to this mechanism and produce gaps exceeding 0.2 eV at coverages as low as 2%. Although our DFT calculations of necessity invoked periodic adatom configurations, our tight-binding simulations indicate that readily observable bulk (mobility) gaps should survive also in the random case relevant for experiments. These findings are expected to greatly facilitate the realization of a TI phase in graphene-based systems. We suspect, however, that the mechanism exposed here has much broader applications since (contrary to Ref. [23]) the physics has nothing to do with the graphene-specific Kane-Mele model. Hybridizing trivial metals or insulators with heavy-element impurity bands may therefore provide a generic method for designing new topological phases, which would be interesting to investigate in future work.

The authors gratefully acknowledge A. Damascelli, J. Eisenstein, J. Folk, E. Henriksen, and C. Zeng for helpful discussions, as well as C. Weeks for performing transport calculations related to this study. This work was supported by DOE Grant No. DE-FG02-05ER46237 (J. H. and R. W.), the National Science Foundation through Grant No. DMR-1055522 (J. A.), the Alfred P. Sloan Foundation (J. A.), NSERC (M. F.), and CIfAR (M. F.).

*aliceaj@caltech.edu
†wur@uci.edu

[1] C. L. Kane and E. J. Mele, Phys. Rev. Lett. **95**, 226801 (2005).
[2] M. Z. Hasan and C. L. Kane, Rev. Mod. Phys. **82**, 3045 (2010).
[3] X.-L. Qi and S.-C. Zhang, Rev. Mod. Phys. **83**, 1057 (2011).
[4] L. Fu and C. L. Kane, Phys. Rev. Lett. **100**, 096407 (2008).
[5] L. Fu and C. L. Kane, Phys. Rev. B **79**, 161408 (2009).
[6] C. W. J. Beenakker, arXiv:1112.1950.
[7] J. Alicea, Rep. Prog. Phys. **75**, 076501 (2012).
[8] B. Seradjeh, J. E. Moore, and M. Franz, Phys. Rev. Lett. **103**, 066402 (2009).
[9] X.-L. Qi, T. L. Hughes, and S.-C. Zhang, Phys. Rev. B **78**, 195424 (2008).
[10] A. M. Essin, J. E. Moore, and D. Vanderbilt, Phys. Rev. Lett. **102**, 146805 (2009).
[11] Q. Meng, V. Shivamoggi, T. L. Hughes, M. J. Gilbert, and S. Vishveshwara, Phys. Rev. B **86**, 165110 (2012).
[12] L. Jiang, D. Pekker, J. Alicea, G. Refael, Y. Oreg, A. Brataas, and F. von Oppen, arXiv:1206.1581.
[13] N. Nagaosa, Science **318**, 758 (2007).
[14] B. A. Bernevig, T. L. Hughes, and S.-C. Zhang, Science **314**, 1757 (2006).
[15] M. Konig, S. Wiedmann, C. Brune, A. Roth, H. Buhmann, L. W. Molenkamp, X.-L. Qi, and S.-C. Zhang, Science **318**, 766 (2007).
[16] A. Roth, C. Brune, H. Buhmann, L. W. Molenkamp, J. Maciejko, X.-L. Qi, and S.-C. Zhang, Science **325**, 294 (2009).
[17] C. Brune, A. R. H. Buhmann, E. M. Hankiewicz, L. W. Molenkamp, J. Maciejko, X.-L. Qi, and S.-C. Zhang, Nat. Phys. **8**, 486 (2012).
[18] I. Knez, R.-R. Du, and G. Sullivan, Phys. Rev. Lett. **107**, 136603 (2011).
[19] S. Raghu, X.-L. Qi, C. Honerkamp, and S.-C. Zhang, Phys. Rev. Lett. **100**, 156401 (2008).
[20] C. Weeks and M. Franz, Phys. Rev. B **81**, 085105 (2010).
[21] T. Pereg-Barnea and G. Refael, Phys. Rev. B **85**, 075127 (2012).
[22] N. H. Lindner, G. Refael, and V. Galitski, Nat. Phys. **7**, 490 (2011).
[23] C. Weeks, J. Hu, J. Alicea, M. Franz, and R. Wu, Phys. Rev. X **1**, 021001 (2011).
[24] D. Xiao, W. Zhu, Y. Ran, N. Nagaosa, and S. Okamoto, Nat. Commun. **2**, 596 (2011).
[25] M. S. Miao, Q. Yan, C. G. Van de Walle, W. K. Lou, L. L. Li, and K. Chang, Phys. Rev. Lett. **109**, 186803 (2012).
[26] P. Ghaemi, S. Gopalakrishnan, and T. L. Hughes, Phys. Rev. B **86**, 201406(R) (2012).
[27] D. Huertas-Hernando, F. Guinea, and A. Brataas, Phys. Rev. B **74**, 155426 (2006).
[28] H. Min, J. E. Hill, N. A. Sinitsyn, B. R. Sahu, L. Kleinman, and A. H. MacDonald, Phys. Rev. B **74**, 165310 (2006).
[29] Y. Yao, F. Ye, X.-L. Qi, S.-C. Zhang, and Z. Fang, Phys. Rev. B **75**, 041401 (2007).
[30] J. C. Boettger and S. B. Trickey, Phys. Rev. B **75**, 121402 (2007).
[31] M. Gmitra, S. Konschuh, C. Ertler, C. Ambrosch-Draxl, and J. Fabian, Phys. Rev. B **80**, 235431 (2009).
[32] O. Shevtsov, P. Carmier, C. Groth, X. Waintal, and D. Carpentier, Phys. Rev. B **85**, 245441 (2012).
[33] H. Jiang, Z. Qiao, H. Liu, J. Shi, and Q. Niu, Phys. Rev. Lett. **109**, 116803 (2012).
[34] Z. Qiao, S. A. Yang, W. Feng, W.-K. Tse, J. Ding, Y. Yao, J. Wang, and Q. Niu, Phys. Rev. B **82**, 161414 (2010).
[35] H. Zhang, C. Lazo, S. Blügel, S. Heinze, and Y. Mokrousov, Phys. Rev. Lett. **108**, 056802 (2012).
[36] L. Fu and C. L. Kane, Phys. Rev. B **76**, 045302 (2007).
[37] See Supplemental Material at http://link.aps.org/supplemental/10.1103/PhysRevLett.109.266801 for further discussion of the Z_2 invariant and additional DFT results.
[38] C. Weeks (unpublished).
[39] G. Kresse and J. Furthmuller, Comput. Mater. Sci. **6**, 15 (1996).
[40] G. Kresse and J. Furthmuller, Phys. Rev. B **54**, 11169 (1996).
[41] J. P. Perdew and A. Zunger, Phys. Rev. B **23**, 5048 (1981).
[42] K. T. Chan, J. B. Neaton, and M. L. Cohen, Phys. Rev. B **77**, 235430 (2008).
[43] X. Liu, C. Z. Wang, Y. X. Yao, W. C. Lu, M. Hupalo, M. C. Tringides, and K. M. Ho, Phys. Rev. B **83**, 235411 (2011).
[44] O. V. Yazyev and A. Pasquarello, Phys. Rev. B **82**, 045407 (2010).
[45] W. Tang, E. Sanville, and G. Henkelman, J. Phys. Condens. Matter **21**, 084204 (2009).